To appear in the *Geophysical Research Letters*, 1998.

The outer radiation belt during the 10 January, 1997 CME event

P. Bühler, L. Desorgher, and A. Zehnder
Paul Scherrer Institut, Villigen PSI, Switzerland

A. Johnstone
Mullard Space Science Laboratory, University College London, Holmbury St.Mary, United Kingdom

E. Daly and L. Adams
ESTEC, Noordwijk, The Netherlands

Abstract

On 10 January 1997 a magnetic cloud of a coronal mass ejection impinged upon the earth magnetosphere and caused considerable variations of the relativistic electron population in the earth's outer radiation belt in the following days. Data obtained with radiation detectors on board a pair of satellites, STRV-1a and STRV-1b in a nearly equatorial geostationary transfer orbit show that the electron flux variations during the days following the arrival of the magnetic cloud can be characterized by four phases during which the fluxes alternatingly decreased and increased. The close relation between flux and Dst variations suggest the magnetic field variations in the inner magnetosphere to play an important role. However, the observed injection of electrons into the trapping region in the morning of 10 January seems to be crucial for the large electron flux enhancement during the afternoon of 10 January.

Introduction

The high energetic electron population in the earth's outer radiation belt is highly dynamic. Although it has been known for a long time, that major variations of the outer radiation belt are associated with solar wind disturbances [*Williams,* 1966], the coupling mechanism between solar wind and trapped particles is not well understood. It has been shown, that on a statistical basis the relativistic electron flux enhancements which normally occur during such events tend to increase with the solar wind velocity and are promoted by a southward turning of the Interplanetary Magnetic Field, IMF [*Paulikas and Blake,* 1979]. But the source or acceleration process leading to those enhancements has not been clearly identified. Recently Li et al. (1997) showed that the number of energetic electrons in the solar wind is not sufficient to be the main source for the outer radiation belt electrons.

On 10 January 1997 a magnetic cloud from a Coronal Mass Ejection, CME hit the earth and produced considerable variations of the high energy electrons in the outer radiation belt. A pair of microsatellites STRV-1a and -1b [*Wells,* 1994] were launched in June 1994 as secondary attached payloads to an Ariane 4 vehicle and carried a number of instruments for monitoring the radiation environment including the Radiation Environment Monitor, REM [*Bühler et al.,* 1996] on STRV-1b and the Cold Ion Detector, CID [*Papatheodorou et al.,* 1997] on STRV-1a. In this paper we present relativistic electron data from the two instruments and discuss possible processes leading to the observed variations.

Instrument

The two STRV spacecraft were launched together and placed into geostationary transfer orbit with a period of 10.5 hrs, and with an inclination of 7°. During this event, the times at apogee for the two orbits were only 20 minutes apart so the orbits are virtually in step. The local time of apogee was between 5.6 hrs MLT and 6.0 hrs MLT.

STRV-1b carried the REM instrument from the Paul Scherrer Institut which measures the energy deposit of high energy electrons and protons in two independent, shielded solid state detectors. The lower energy threshold for particles to be detected is approximately 1 MeV for electrons and 25 MeV for protons. Energy deposits are measured and accumulated into two 16-bin histograms. The accumulation time varies with spacecraft position and is 100 sec below L≈4.5 and 1000 sec near apogee. In view of the rather large aperture of 90°, the long accumulation time and the fact that the satellite spins with a rate of approximately 6 rpm, REM is assumed to measure omnidirectional fluxes. In this paper we only discuss REM data in the outer belt at L≥3. There the count rates are dominated by electrons and the contribution of > 25 MeV protons can be neglected.

STRV-1a carried a dual retarding potential analyser, the Cold Ion Detector, CID to measure ambient cold ions. Penetrating electrons and ions generated background noise which could be separated from the ion measurements in a special measurement. The detector was a microchannel plate surrounded by a sleeve of insulator inside an aluminium tube with 2 mm thick walls. The amount of shielding is slightly less than the absorber around the REM detector making it sensitive to electrons below 1 MeV. The instrument was aligned with the spacecraft spin axis and like REM it's effective field of view is large. Therefore it also measures omnidirectional fluxes. The CID samples are snapshots of the flux at approximately 5 minute intervals rather than the longer accumulations used by REM.

Observations

We focus on the three days from 10 January to 13 January 1997. In figure 1 the solar wind velocity and density from the Solar Wind Experiment aboard Wind [*Ogilvie et al.,* 1995] and B_z, the IMF z-component [*Lepping et al.,* 1995] are plotted together with the geomagnetic activity index Dst. The vertical lines mark the times when the REM detectors passed through the outer radiation belt at L=5.

The period under consideration can be characterized by four phases. The first one lasted from the early morning of 10 January until 10 UT and was characterized by a slight increase of the solar wind velocity, the southward turning of the IMF and the development of a medium magnetic storm with a minimum Dst of -80. The second phase lasted until 03 UT on 11 January. During this phase the IMF turned steadily back northward and Dst recovered. The arrival of a high density filament around 01 UT on 11 January made the Dst index jump to positive values, probably due to induced magnetopause currents. The third phase from 03 UT to 13 UT of 11 January was characterized by a further increase of the solar wind velocity, a recovery of B_z and the build up of a weak magnetic storm with minimum Dst of -50. During the

fourth phase which lasted from 13 UT of 11 January for a few days, Dst slowly recovered to its pre-storm value.

Using figures 2 and 3 we follow now what happened with the energetic electron fluxes in the outer belt during these four phases. The eleven panels in figure 2 show the REM count rates as function of L for the different outer radiation belt passes marked in figure 1. In order to facilitate the comparison between successive passes, in each panel the previous pass is plotted as dotted line. In the right upper corner of each panel the measured peak rate is also given.

The CID data are shown in a contrasting way in figure 3. The data are plotted orbit by orbit on a time scale which runs from perigee to perigee centred on the apogee time. Such a display takes advantage of the better time resolution of CID near apogee and allows the timing of events seen at STRV-1a to be compared with other observations. The orbits of STRV-1a are numbered with respect to the first mentioned. The data were not recorded from all orbits.

During the first part of January 1997 geomagnetic activity and the electron intensity in the radiation belts were both very low. Two days before the magnetic cloud engulfed the earth the CID count rates (CID-orbit 1) as well as the REM rates (not shown here) were well below average intensity. Whereas the CID rates showed a broad maximum around L=5.9 the REM rates showed a double peaked distribution in L space with an inner peak centered at L≈3.3 and an outer peak at L≈4.0. The difference is probably a manifestation of the lower CID energy threshold compared to REM.

The REM rates hardly changed during REM-pass 1. On the following inbound-leg (REM-pass 2) the count rates at L>5 had increased by roughly a factor 2. Below L=5 the count rates were lower than during the previous pass. The peak at L=4 had disappeared while the peak at L=3.3 had changed slightly. CID data with their enhanced temporal resolution reveal more details. During CID-orbit 5 the count rates followed the profile measured during orbit 1 until the first sign of change at 04:00 UT at L=6.2, when the intensity stayed level instead of decreasing. Then at 04:38 UT, L=6.55, the intensity increased sharply by a factor of 2.8. Almost as sharply it dropped again to the orbit 1 baseline. Strong substorm activity which started just after 04:00 UT was responsible for the injection at 04:38 UT but the simultaneous rapid decrease in Dst to -80 nT probably made the electron intensity return to baseline. On the inbound-leg, new substorm-related injection peaks at 07:13 UT, L=6.35, were followed by two drift echoes whose timing corresponds to approximately 0.5 MeV electrons. In contrast to REM, CID observes sustained increases by a factor 6 in electron intensities down to L=3.6 before 10:00 UT.

During REM passes 3 to 5, which correspond in time with the Dst increase, a strong electron flux enhancement was observed. The new distribution peaked first at L=5.1 but then moved inward. From pass 2 to pass 5 the maximum count rate went up by a factor 200 and the peak position moved inward to L=4.8. Dst reached its maximum value of +50 nT at 02:00 UT on the 11th when the two spacecraft were close to apogee. Between 01:17 and 02:23 UT the CID observed a drop out in the electron fluxes (outbound-leg CID-orbit 7) at L≈6.6. Related events included an increase by 50 nT in the magnetic field at GOES-9, on the opposite side of the magnetosphere near dusk, and a magnetopause crossing by the LANL-94 geosynchronous spacecraft [*Reeves et al.,* 1997]. A similar flux dropout in relativistic electrons was observed by other LANL spacecraft.

During the following pass (REM-pass 6, inbound-leg of CID-orbit 7) both detectors showed a further increase of the peak intensity by a factor 1.6 and a significant inward shift of the peak position to L=4.4. The inward movement of the particle distribution is probably the response to the high solar wind density peak. The induced electric field produced by the magnetic field compression at the arrival of a solar wind pressure pulse can accelerate electrons and move them inward [*Li et al.,* 1993].

Following the passage of the solar wind pressure pulse, Dst decreased again and the radiation belts changed in response. Both instruments (REM-passes 7 & 8, CID-orbit 8) observed decreasing fluxes during the following orbit. The decrease was most significant at large L. Around apogee the CID rates even fell to their pre-storm level. The peak position remained at L=4.4. At 11:15 UT, STRV-1a was at L=6.85 and local time 5.6 hr making it possibly the closest spacecraft to Telstar 401 at the time of its failure. Yet at this time the energetic electron intensity it measured was at the lower-than-average pre-storm level.

In the inner part of the next available CID orbit (CID-orbit 10) the intensity practically followed the orbit 8 level with only slightly increased flux. Beyond L=6, a series of injection events were registered by CID and the electron intensity rose again essentially filling in the hole formed in orbit 8 but not to the level

of orbit 7. The injection events occur together with a negative feature in the IMF z-component and Dst. Enhanced rates especially at L>6 were also observed by REM during pass 12.

During REM pass 13 the rates had further slightly increased. From then on however, the peak rate slowly decayed and the peak position continued to slowly move inward until it was interrupted on 17 January, when a new solar wind enhancement arrived and caused a new disturbance. By 17 January the peak position had moved down to L=4.2.

Discussion

The fact that the temporal evolution of the flux variations follow the Dst and B_z variations closely suggests that the magnetic field variations play an important role. During phase one when Dst dropped the REM count rates below L=4.5 decreased. At larger L and lower energies (CID), where at the same time the rates increased, the effect of the magnetic field variation was probably dominated by the injection of lower energy particles clearly seen in the CID data. During phase two when Dst recovered the electron fluxes strongly increased, then decreased together with Dst during phase three and slightly increased again during the first part of the final recovery phase.

A similar correlation is found for the variations of the electron spectra. As a measure for the electron spectra we plot in figure 4 a hardness ratio averaged over $4.5 \leq L \leq 5.5$. It is the count rate ratio between two REM channels with approximate energy thresholds of 1.5 MeV and 2.0 MeV. A high hardness ratio signifies a soft spectrum, a low value a hard spectrum. A ratio of 3 corresponds to an exponential differential energy spectrum ($f(E) \propto e^{-\gamma_{exp}E}$ in units of $cm^{-2}sec^{-1}MeV^{-1}$) with a spectral index γ_{exp} of approximately 3, and a ratio of 4 to a γ_{exp} of approximately 3.5. During phases one and three, when Dst decreased, the spectra softened and during the phases two and four, when Dst increased the spectra hardened.

The major magnetic field variations during the magnetic storm were slow and therefore it can be assumed that the first adiabatic invariant was conserved. In this case the particle energy decreases with the magnetic field. If the third adiabatic invariant is conserved, particles move outward where the magnetic field is even weaker and they lose more energy [*McIlwain,* 1966]. For a detector with fixed detection threshold the deceleration of the particles results in a decreased detection rate .

Besides a change in count rate also a change of the particle spectrum can be expected. To demonstrate the effect we calculated the ratio between initial and final energy spectra at a given location as function of the relative local magnetic field change $\Delta B/B$, where B is the magnetic field strength before and B-ΔB the magnetic field strength after the magnetic change. The calculations are restricted to equatorially mirroring particles and assume phase space density to be independent of L. The last assumption makes the ratio to only depend on the local field variation which considerably simplifies the calculation. The radial movement of the particles does not have to be traced and no further assumptions about the magnetic field have to be made.

The results are shown in figure 5. The solid lines show results for an exponential energy spectrum with a spectral index $\gamma_{exp} = 2.5$ and the dotted line the results for an initial spectrum with a $\gamma_{exp} = 3.5$, respectively, typical values for the quiet time relativistic electron spectra in the outer radiation belt.

The calculations demonstrate that a magnetic field decrease can result in a flux drop at energies above 1 MeV and a significant softening of the spectrum and visa versa. Note, that the results strongly depend on the initial spectral shape and that it is the relative and not the absolute magnetic field variation which determines the strength of the effect.

In reality phase space density is not homogeneous [*Selesnick and Blake,* 1997] which has to be taken into account for a detailed comparison with the data. Generally it can be noted that a positive slope of the phase space density distribution in L-space would rather increase the effect whereas a negative slope would weaken it.

Although the magnetic field effect is important the injection of particles during the early morning of 10 January is probably most crucial for the occurrence of the strong flux increase during phase two. The CID data show that by 12:00 UT when Dst started to increase the inner magnetosphere down to L≈3.6 had been filled with <1 MeV electrons. During the recovery phase these particles must have been accelerated by the recovery of the magnetic field and at least partly contributed to the observed flux enhancement at higher energies. In order to quantify the contribution of the magnetic field effect to the observed flux enhancement, a better estimate of the involved parameters (e.g. phase space density) would be needed. Additional acceleration processes are not excluded.

The fact that the new relativistic electron flux distribution peaks first around L=5 is a common feature of the storm time behavior of the relativistic electron population and was often observed with REM during magnetic storms [*Desorgher et al.,* 1996]. Although this does not necessarily imply the acceleration process to be localized at L=5 it is interesting to note that available dynamic external magnetic field models [*Olson and Pfitzer,* 1982; *Tsyganenko,* 1989] together with the static IGRF predict the local $\Delta B/B$ value during magnetic storms to be maximum around L=5 along the STRV orbit (in this case B was calculated using IGRF 95 + external field model with quiet time parameters Kp=0, Dst=0, ρ=25 cm^{-3}, SWV=300 km/sec and B-ΔB using IGRF 95 + external field model with Kp=6, Dst=-80, ρ=25 cm^{-3}, and SWV=450 km/sec). However, whether the flux distribution after such a magnetic field change would peak at the same position does mainly depend on the phase space density distribution of the particles which are accelerated.

The slow inward motion of the count rate distribution and the smooth decay of the count rates during the last phase suggest that radial and pitch angle diffusion are active as well. Although adiabatic acceleration continues during the whole recovery phase, the electron flux slowly begins to decrease after a few days, presumably due to pitch angle diffusion.

Conclusion

Relativistic electron flux and spectral variations observed in the earth's outer radiation belt during the 10 January CME event correlate well in time with the observed Dst and IMF variations, suggesting magnetic field variations to be one of the important driving parameters for the trapped relativistic electrons. If adiabatic magnetic variations were the only process acting on the relativistic electrons the flux before and after the storm would be the same, which is clearly not the case. However, the CID observations show that the necessary seed population of lower energy particles, which could have been accelerated in the second half of 10 January to energies exceeding 1 MeV was provided by an injection event, just before Dst started to increase.

Acknowledgments. We gratefully acknowledge the work done by D.J. Rodgers to establish the comparability of the two data sets. The work on the REM detector was supported by ESA/ESTEC/WMA Technology Research Contract 11108/94/NL/JG(SC). The work on the CID detector was supported by the UK Defense Evaluation and Research Agency.

References

Bühler, P. et al., Radiation Environment Monitor, *Nucl. Instr. and Meth. in Phys. Res. A, 386,* 825, 1996

Desorgher, L. et al., Variations of the outer radiation belt during the last two years, *esa SP-392,* 137, 1996

Lepping, R. P. et al., The WIND magnetic field investigation, *Space Sci. Rev., 71,* 207, 1995

Li, X. et al., Simulation of the prompt energization and transport of radiation particles during March 23, 1991 SSC, *Geophys. Res. Lett., 20,* 2423, 1993

Li, X. et al., Are energetic electrons in the solar wind the source of the outer radiation belt?, *Geophys. Res. Lett., 24,* 923, 1997

McIlwain, C. E., Ring current effects on trapped particles, *J. Geophys. Res., 71,* 3623, 1966

Ogilvie, K. W. et al., SWE, a comprehensive plasma instrument for the Wind spacecraft, *Space Sci. Rev., 71,* 55, 1995

Olson, W. P. and Pfitzer, K. A., A dynamic model of the magnetospheric magnetic and electric fields for July 29, 1977, *J. Geophys. Res., , 87,* 5943, 1982

Paulikas, G. A. and Blake, J. B., Effects of the solar wind on magnetospheric dynamics: energetic electrons at the synchronous orbit, *Geophys. Monograph Series 21,* 181, 1979

Papatheodorou, et al., A miniature plasma analyser with a differential energy response, *Measurement Techniques for Space Plasmas,* Geophys. Monograph Series, submitted 1996.

Reeves, G. D. et al., The relativistic electron response at geosynchronous orbit during the January 1997 magnetic storm, *J. Geophys. Res., ,* submitted, 1997.

Selesnick, R. S. and Blake, J. B., Dynamics of the outer radiation belt, *Geophys. Res. Lett., 24,* 1347, 1997

Tsyganenko, N. A., A magnetospheric magnetic field model with a warped tail current sheet, *Planet. Space. Sci., 37,* 5, 1989

Wells, N, The Space Technology Research Vehicles STRV–1A and STRV–1B: First in–orbit results, 8th annual AIAA/Utha State University Conference on small satellites, 1994

Williams, J., A 27-day periodicity in outer zone trapped electron intensities, *J. Geophys. Res., 71,* 1815, 1966

September 24, 1997; revised January 13, 1998; accepted January 23, 1998.

This preprint was prepared with AGU's LaTeX macros v4. File jan1097˙paper formatted February 14, 1998.

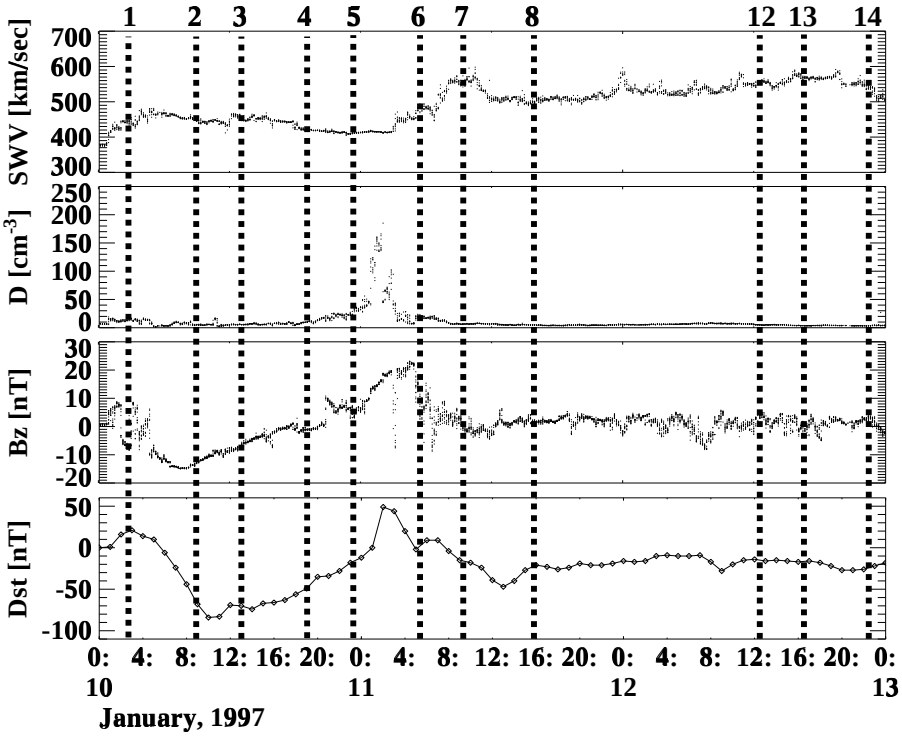

Figure 1. Solar wind velocity, solar wind density, IMF z-component, and Dst from 10 to 13 January 1997. The vertical lines mark the times when REM passed at L=5.

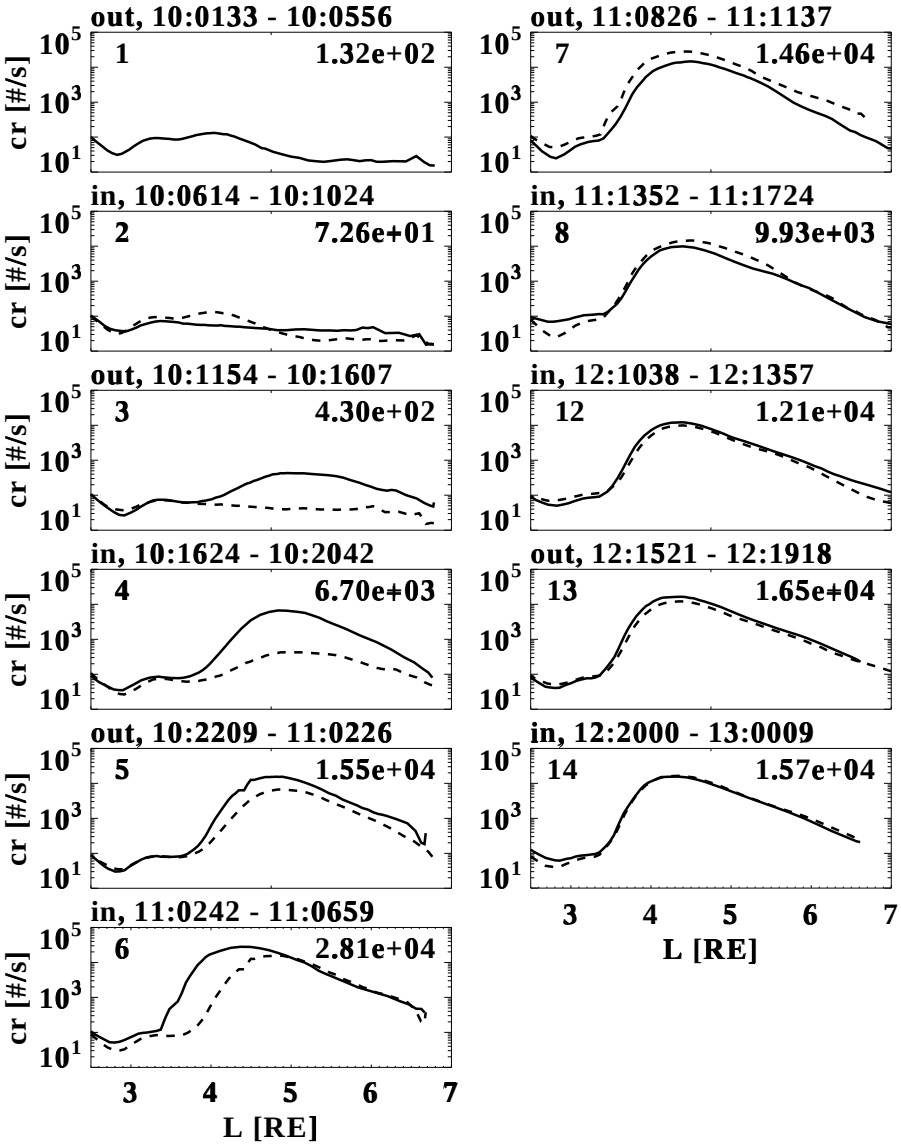

Figure 2. REM passes through the outer radiation belt from 10 to 13 January 1997. In order to facilitate the comparison between successive passes, in each panel the previous pass is shown as dotted line. In the upper right corner of each panel the peak count rate is given.

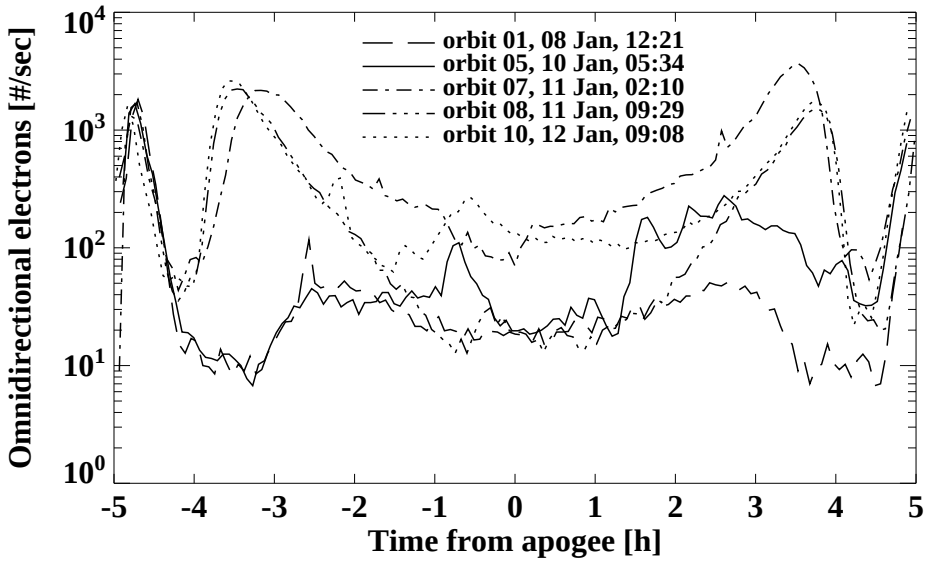

Figure 3. CID count rates versus time during different orbits.

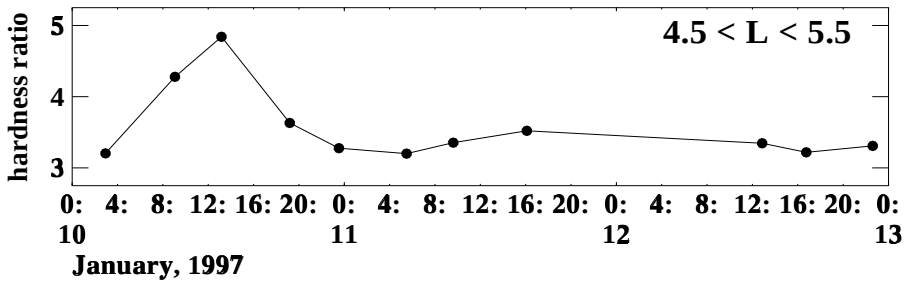

Figure 4. Hardness ratio of the electron energy spectrum at L=5. High ratios signify soft spectra, low ratios hard spectra (see text for more details).

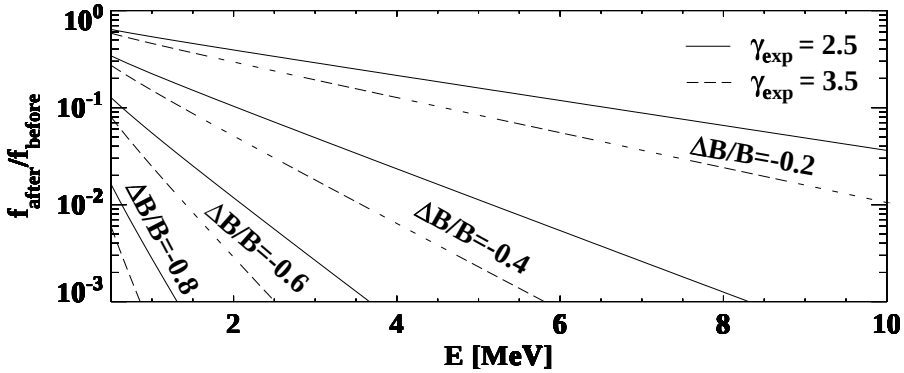

Figure 5. Ratio between differential electron spectra after and before adiabatic deceleration at a given spatial location for four values of the relative local magnetic field variation $\Delta B/B$. The calculations assume phase space density to be independent of L which makes the ratio to only depend on the local field variation. Solid lines are for an initial exponential spectrum with a spectral index of 2.5 and dotted lines for an initial spectrum with a spectral index of 3.5.